Density Matrix Implementation of the Fermi-Löwdin Orbital Self-interaction Correction Method

Juan I. Melo,[†,‡] Mark R. Pederson,[¶] and Juan E. Peralta[*,§]

†*Universidad de Buenos Aires, Facultad de Ciencias Exactas y Naturales, Departamento de Física. Buenos Aires, Argentina.*

‡*CONICET - Universidad de Buenos Aires, Instituto de Física de Buenos Aires (IFIBA). Buenos Aires, Argentina.*

¶*Department of Physics, the University of Texas at El Paso, El Paso, Texas 79968, USA*

§*Department of Physics, Central Michigan University, Mount Pleasant, MI, 48859, USA*

E-mail: juan.peralta@cmich.edu

Abstract

The Fermi-Löwdin orbital self-interaction correction (FLOSIC) method effectively provides a transformation from canonical orbitals to localized Fermi-Löwdin orbitals which are used to remove self-interaction error in the Perdew-Zunger (PZ) framework. This transformation is solely determined by a set of points in space, called Fermi-Löwdin descriptors (FODs), and the occupied canonical orbitals or the density matrix. In this work we provide a detailed workflow for the implementation of the FLOSIC method for removal of self-interaction error in DFT calculations in an orbital-by-orbital basis that takes advantage of the unitary invariant nature of the FLOSIC method. In this way, it is possible to cast the self-consistent energy minimization at fixed FODs in the same manner than standard Kohn-Sham with one additional term in

the Kohn-Sham Hamiltonian that introduces the PZ self-interaction correction. Each energy minimization iteration is divided in two sub-steps, one for the density matrix and one for the FODs. Expressions for the effective Kohn-Sham matrix and FOD gradients are provided such that its implementation is suitable for most electronic structure codes. We analyze the convergence characteristics of the algorithm and present applications for the evaluation of NMR shielding constants and real-time time-dependent DFT simulations based on the Liouville–von Neumann equation to calculate excitation energies.

1. Introduction

Density functional theory (DFT)[1,2] can be considered the workhorse of electronic structure methods, offering a good compromise between accuracy and computational cost for a wide range of systems and properties.[3–7] Despite its success, DFT is not free from limitations. One of the most striking shortcomings of approximate exchange-correlation density functionals is that they do not completely cancel the interaction of electrons with themselves, giving place to the well-known self-interaction error (SIE). The presence of SIE has been linked to several negative consequences, such as, for example, an incorrect potential energy disociation curve for $H_2{}^+$,[8,9] an underestimation of energy band gaps,[10] and unphysical Kohn-Sham orbitals and orbital energies,[11] which are known to impact calculated magnetic properties.[12]

Perdew and Zunger proposed a scheme to explicitly remove the one-electron SIE[13] on an orbital-by-orbital basis. This scheme, commonly known as PZ-SIC, is based on a modified energy expression,

$$E_{\text{DFT-SIC}} = E_{\text{DFT}}[n^{\uparrow}, n^{\downarrow}] - \sum_{i,\sigma} (E_{\text{XC}}[n_i^{\sigma}, 0] + E_{\text{H}}[n_i^{\sigma}]) \,, \tag{1}$$

where n_i^{σ} are single orbital spin densities ($\sigma = \uparrow, \downarrow$) and E_{XC} and E_{H} are the exchange-correlation and Hartree energies, respectively. The PZ scheme to remove SIE delivers the

proper corrections to approximate density functionals *via* localized orbitals. However, this scheme has not been adopted for routine applications due to the high computational cost associated with solving a system of equations, also known as the localization equations,[14] which involves finding a unitary transformation that minimizes $E_{\text{DFT-SIC}}$. In addition to the computational burden involved in removing SIE, its use in combination with standard approximate functionals may be detrimental for many properties, and thus demands careful construction of density functionals for SIC.[15–21]

In the past years, a method for removing the SIE based on the construction of Fermi-Löwdin orbitals (FLOSIC) was proposed.[22–24] Within this approach, the localized orbitals that are used for minimizing $E_{\text{DFT-SIC}}$ are parametrized in the form of Fermi orbitals[25] $f_a(\mathbf{r})$,

$$f_a(\mathbf{r}) = \frac{\sum_\alpha \psi^*_\alpha(\mathbf{a})\psi_\alpha(\mathbf{r})}{\sqrt{n(\mathbf{a})}}\,, \tag{2}$$

where $\mathbf{a}$ are points in space, called Fermi orbital descriptors (FODs), $\psi_\alpha(\mathbf{r})$ are the canonical Kohn-Sham orbitals which define the occupied sub-space, n is the electron density, and a denotes an FOD label. The spin indices have been omitted for clarity. The non-orthogonal Fermi orbitals $f_a(\mathbf{r})$ are then orthogonalized using the Löwdin orthogonalization scheme[26] to give place to the Fermi-Löwdin localized orthonomal orbitals (FLOs), which are solely determined by the occupied manifold and the set of FODs. Minimizing $E_{\text{DFT-SIC}}$ therefore involves relaxing the canonical orbitals (or the occupied sub-space) *and* the FODs. In the original implementation of the FLOSIC method in the FLOSIC code[27], the occupied sub-space relaxation was achieved by means of Jacobi-type rotations to zero the overlap between the occupied and virtual orbitals at each self-consistent iteration, much like traditional implementations of Foster-Boys,[28,29] Edmiston-Ruedenberg,[30] or Pipek-Mezey[31] localization schemes. Other implementations of FLOSIC are based on unified Hamiltonian schemes and effective potentials.[32–36] In this work we introduce an implementation of FLOSIC based on the minimization of $E_{\text{DFT-SIC}}$. An effective mean-field Kohn-Sham Hamiltonian, including

self-interaction, is derived as a derivative of $E_{\text{DFT-SIC}}$ with respect to the 1-particle density matrix, leading to a set of standard self-consistent Roothaan-Hall equations that determine the occupied orbitals and hence the density matrix. The set of FODs is relaxed in a separate step to complete a fully variational procedure for the minimum of $E_{\text{DFT-SIC}}$.

2. Theory and Implementation

Since the set of Fermi orbitals defined in eq. (2) is a normalized but not orthogonal set, a Löwdin symmetric orthogonalization is performed to give Fermi-Löwdin orbitals (FLOs),

$$F_a(\mathbf{r}) = \sum_b [\mathbf{O}^{-1/2}]_{ab} f_b(\mathbf{r}) \,, \tag{3}$$

with

$$\mathrm{O}_{ab} = \frac{\sum_\alpha \psi^*_\alpha(\mathbf{a})\psi_\alpha(\mathbf{b})}{\sqrt{n(\mathbf{a})n(\mathbf{b})}} \tag{4}$$

the Fermi orbital overlap matrix. This choice of orthogonalization ensures that the Fermi orbitals and FLOs are as close as possible, in the least-squares sense.[37] The transformation from Fermi-orbitals to Fermi-Löwdin orbitals and its inverse have been derived in Ref. 38. The FLOs depend only on the FODs and the occupied canonical orbitals, and therefore it is possible to write the single-orbital Fermi-Löwdin densities $\mathbf{P}_a$ in terms of the total density matrix $\mathbf{P}$ and the FODs (vide infra). This allows us to write the Perdew-Zunger energy in terms of the total density matrix and the FODs,

$$E_{\text{DFT-SIC}}(\mathbf{P}, \{\mathbf{a}\}) = E_{\text{DFT}}(\mathbf{P}) + E_{\text{SIC}}(\mathbf{P}, \{\mathbf{a}\}), \tag{5}$$

with

$$E_{\text{SIC}}\big(\mathbf{P}, \{\mathbf{a}\}\big) = -\sum_a E_{\text{HXC}}(\mathbf{P}_a) \,. \tag{6}$$

In eq. (6), E_{HXC} is the Hartree plus exchange-correlation energy. Finding a stationary

solution of $E_{\text{DFT-SIC}}$ in eq. (5) with the standard constraints of orbital orthonormalization leads to the Kohn-Sham equations, and the only difference between standard Kohn-sham and Perdew-Zunger in this case is the additional $E_{\text{SIC}}(\mathbf{P}, \{\mathbf{a}\})$ term, which accounts for removal of self-interaction and depends on $\mathbf{P}$ and all the FODs. Thus, for a given (fixed) set of FODs, the effective KS Hamiltonian is

$$\mathbf{H}_{\text{KS}} = \frac{dE_{\text{DFT-SIC}}}{d\mathbf{P}} = \frac{dE_{\text{DFT}}}{d\mathbf{P}} + \frac{dE_{\text{SIC}}}{d\mathbf{P}}\,, \tag{7}$$

where

$$\frac{dE_{\text{SIC}}}{d\mathbf{P}} = \sum_a \frac{dE_{\text{SIC}}}{d\mathbf{P}_a} \cdot \frac{d\mathbf{P}_a}{d\mathbf{P}}\,. \tag{8}$$

Equations (5) and (7) provide the energy and an effective "mean-field" Hamiltonian that includes the self-interaction correction. In eq. (8), the "$\cdot$" symbol represents contraction on all the indices of $\mathbf{P}_a$. The solutions of the KS equations using the augmented $\mathbf{H}_{\text{KS}}$ given in eq. (7) can be obtained using very well-developed self-consistent techniques, available for standard KS calculations. However, it should be pointed out that this Hamiltonian does not provide the fully variational solution because it does not allow for FOD relaxation. In practice, relaxation of both, FODs and density matrix can be performed using a two-loop self-consistency as suggested by Lehtola et al.[39] In our approach, the density matrix and FODs are relaxed in independent steps, which are repeated until convergence of all parameters is achieved, as shown schematically in Figure 1. This double loop strategy has been successfully used in several implementations of SIC methods.[32,33,39]

The mean-field Hamiltonian in eq. (7) is derived from variations of the total energy, and hence the self-consistent solutions of the KS equations with SIC provide a stationary solution of the energy in eq. (5) at fixed FODs. The matrix elements of the single-orbital density matrices $\mathbf{P}_a$, needed for the evaluation of $E_{\text{DFT-SIC}}$ in eq. (5), can be obtained following three simple steps:

1. Evaluate the transformation matrix $\mathbf{G}$ from atomic orbitals (AOs) $\phi_\nu(\mathbf{r})$ to Fermi-

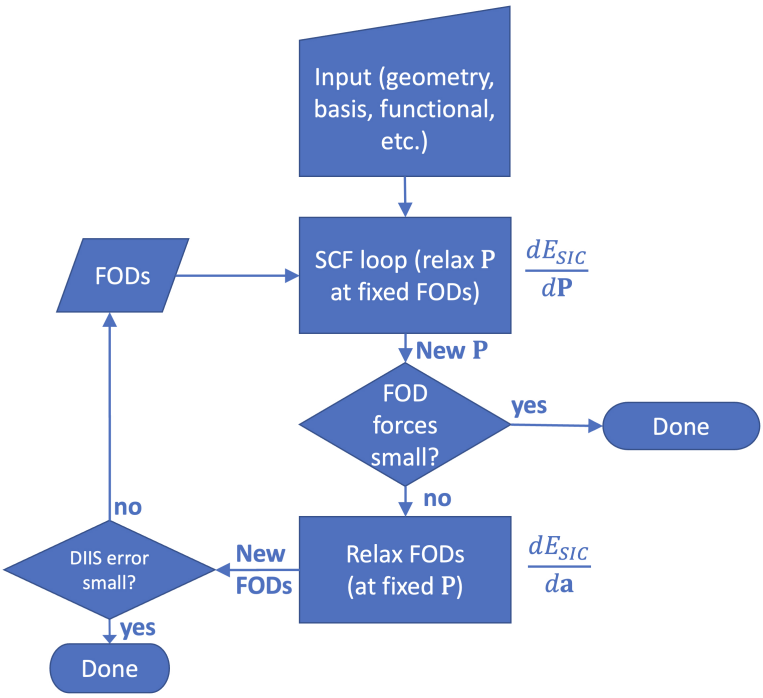

Figure 1: Flowchart of the algorithm used for FLOSIC calculations.

orbitals $F_a(\mathbf{r})$ as $G_{\nu a} = \sum_\mu Q^a_{\mu\nu}$, where $Q^a_{\mu\nu} = P_{\mu\nu}\phi_\mu(\mathbf{a})/\sqrt{n(\mathbf{a})}$.

2. Calculate the Fermi-orbital overlap matrix as $\mathbf{O} = \mathbf{G}^\dagger\mathbf{S}\mathbf{G}$ ($\mathbf{S}$ is the AO overlap matrix). Alternatively, the FO overlap can be evaluated as $\mathbf{O} = \mathbf{Y}^\dagger\mathbf{P}\mathbf{Y}$. Where $Y_{\mu a} = \phi_\mu(\mathbf{a})/\sqrt{n(\mathbf{a})}$ and the fact that $\mathbf{P}$ is idempotent ($\mathbf{P} = \mathbf{P}\mathbf{S}\mathbf{P}$) has been used.

3. Using the Fermi-orbital overlap matrix, construct the single-orbital density using $[\mathbf{P}_a]_{\mu\nu} = X^*_{\mu a}X_{\nu a}$, where $\mathbf{X} = \mathbf{G}\mathbf{O}^{1/2}$.

It can be easily verified that $\sum_a \mathbf{P}_a = \mathbf{P}$, consistently with the unitary invariance of the FLOSIC transformation. Additionally, by construction, each $\mathbf{P}_a$ is idempotent and holds exactly one (or two for the closed-shell case) electrons.

During the density matrix relaxation, the additional term needed in $\mathbf{H}_{\mathrm{KS}}$ to account for SIE (eq. (7)) can be obtained as the gradient $\frac{dE_{\mathrm{SIC}}}{d\mathbf{P}}$, while for the FOD relaxation loop, the FOD gradients are calculated as $\frac{dE_{\mathrm{SIC}}}{d\mathbf{a}}$. In what follows, we provide the workflow to evaluate generalized gradients of E_{SIC} in the FLOSIC formalism. To simplify the equations, we use

Newton's notation for these gradients, $[\dot{\cdot}] \equiv d/dP_{\lambda\sigma}$ for derivatives with respect to the density matrix elements, or $[\dot{\cdot}] \equiv d/d\mathbf{a}$ for gradients with respect to Cartesian FOD components:

1. Construct $\dot{\mathbf{Q}}$ using:

$$\dot{Q}^a_{\mu\nu} = \frac{dQ^a_{\mu\nu}}{dP_{\lambda\sigma}} = \frac{\phi_\mu(\mathbf{a})\delta_{\mu\nu,\lambda\sigma}}{n^{1/2}(\mathbf{a})} - \frac{1}{2}\frac{P_{\lambda\sigma}\phi_\lambda(\mathbf{a})\phi_\sigma(\mathbf{a})\phi_\mu(\mathbf{a})}{n^{3/2}(\mathbf{a})} \tag{9}$$

   for the self-consistent field (SCF) loop, or

$$\dot{Q}^a_{\mu\nu} = \frac{dQ^a_{\mu\nu}}{d\mathbf{a}} = \frac{P_{\mu\nu}\nabla_{\mathbf{a}}\phi_\nu(\mathbf{a})}{n^{1/2}(\mathbf{a})} - \frac{1}{2}\frac{\phi_\mu\nabla_{\mathbf{a}}n(\mathbf{a})}{n^{3/2}(\mathbf{a})} \tag{10}$$

   for the FOD relaxation loop. Note that $\dot{Q}^a_{\mu\nu}$ in eq. (9) is not symmetric in μ and ν and it is Hermitian in λ and σ, while $\dot{Q}^a_{\mu\nu}$ in eq. (10) does not have any index symmetry. In eq. (10) it has been assumed that $dQ^a_{\mu\nu}/d\mathbf{b} = dQ^a_{\mu\nu}/d\mathbf{a}\,\delta_{ab}$.

2. From eqs. (9) or (10), evaluate $\dot{G}_{\nu a} = \sum_\mu \dot{Q}^a_{\mu\nu}$, and $\dot{\mathbf{O}} = \dot{\mathbf{G}}^\dagger\mathbf{S}\mathbf{G} + \mathbf{G}^\dagger\mathbf{S}\dot{\mathbf{G}}$.

3. Calculate the derivative of the AO-to-FLO transformation matrix as $\dot{\mathbf{X}} = \dot{\mathbf{G}}\mathbf{W} + \mathbf{G}\dot{\mathbf{W}}$, with $\mathbf{W} = \mathbf{O}^{-1/2}$. The $\dot{\mathbf{W}}$ matrix can be calculated from $\dot{\mathbf{O}}$ using the method described by Chen and Gauss (a full derivation is provided in the SI).[40]

4. From $\dot{\mathbf{X}}$, evaluate the gradients using $[\dot{\mathbf{P}}_a]_{\mu\nu} = \dot{X}^*_{\mu a}\,X_{\nu a} + X^*_{\mu a}\,\dot{X}_{\nu a}$.

We have implemented the scheme described above using the relaxation algorithm shown in Figure 1 in an in-house version of the GAUSSIAN program[41] using calls to PYTHON functions to simplify the implementation. The SCF loop is performed entirely using the Gaussian program and thus takes advantage of all the acceleration techniques available in that code. The FOD relaxation is performed using the limited memory Broyden–Fletcher–Goldfarb–Shanno method (L-BFGS) from NUMPY.

In Figure 2, we show the typical convergence characteristics of the double loop algorithm of Figure 1. The SCF loop has excellent convergence properties, in analogy to standard DFT

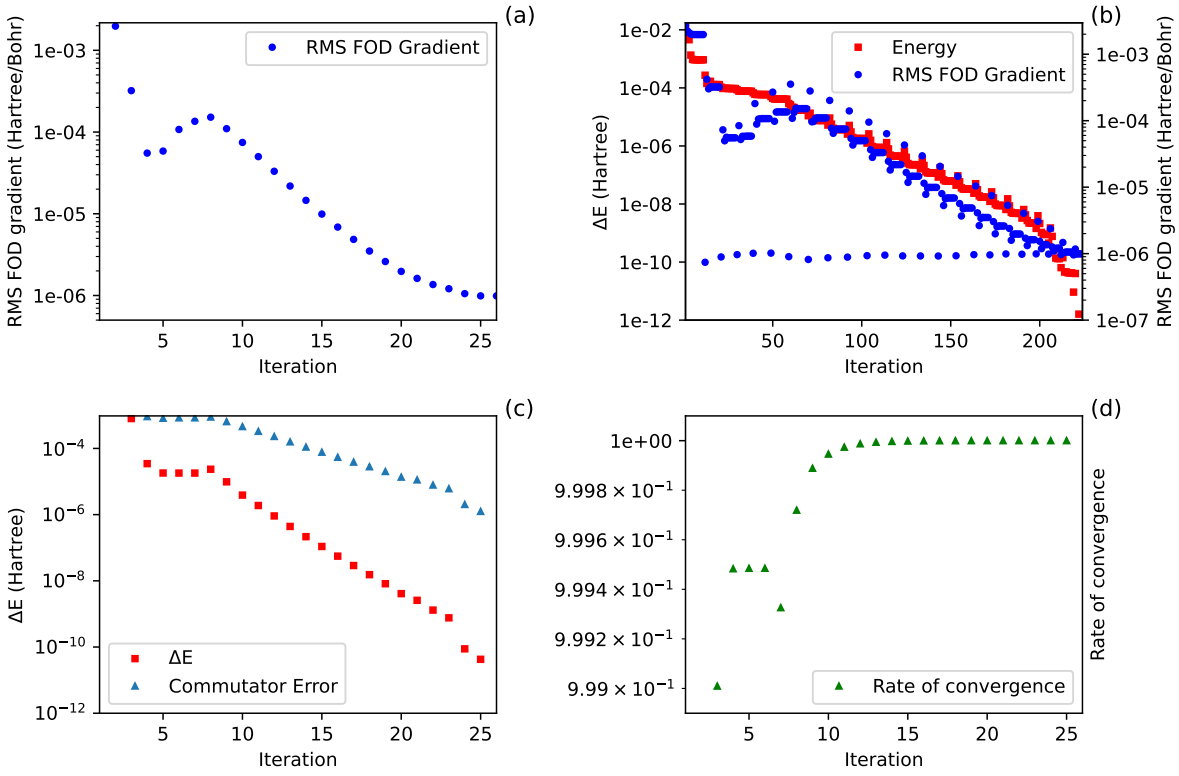

Figure 2: Typical convergence behavior of the optimization algorithm shown in Fig. 1. The plots are for HCN molecule with the aug-cc-pVTZ basis set and the PBE functional. (a) RMS FOD gradient and (c) energy change with respect to the (final) lowest energy at the end of the SCF loop and commutator error (calculated as the norm of $\mathbf{H}_{\mathrm{KS}}\mathbf{PS} - \mathbf{SPH}_{\mathrm{KS}}$) at the beginning of each SCF loop. Panel (b) shows the energy change and RMS FOD gradients at each individual iteration. The blue points in the vicinity of 10^{-6} correspond to the RMS FOD gradient after the FOD relaxation step. Panel (d) shows the rate of convergence of the energy for the entire double-loop algorithm calculated as $|\Delta E_{(n+1)}/\Delta E_n|$, where n is the iteration number.

calculations. The FOD relaxation step was successful in most cases in our tests, provided that a reasonable set of starting FOD is available, with gradients reaching 10^{-6} Hartree/Bohr in a few iterations for small molecules. Fig. 2-a shows the root mean square (RMS) FOD gradient at the end of the SCF loop as a function of the iteration number, with typical values in the range of 10^{-5} to 10^{-6} Ha/Bohr as convergence of the double loop progresses. Fig. 2-b shows both, the RMS FOD gradient and ΔE at each individual SCF cycle. The blue dots that fall below 10^{-6} Ha/Bohr correspond to the first SCF cycle, which evaluate the gradients immediately after the FOD relaxation step. In Fig. 2-c we show the change in energy between two consecutive iterations in the SCF loop, ΔE in Hartree and the commutator error after the FOD relaxation step. The combined double-loop scheme converges only linearly for all the test cases that we performed (see panel d of Figure 2) and highlights one of the potential areas of improvement of the method.

One characteristic of the double-loop optimization is that the FOD energy landscape changes as the occupied manifold changes, unlike in the case of structural relaxation. In Fig. 3, we show the position dependence of the energy and gradients for the C–H bond FOD in the CH_4 molecule. Regardless of being a simple example, Fig. 3 shows some important features of the FOD energy landscape. First, there is a clear basin that hosts the global minimum, as well as three "flat" regions where the FOD gradients become small or zero (Fig. 3-b), potentially causing problems in a gradient-based minimization. Fig. 3-c illustrates a successful optimization case. Starting from the FODs at the leftmost arrow position, the L-BFGS algorithm finds where the gradients are zeroed, at the next arrow to the right. With these new FODs, the SCF procedure determines a new density, which in turn changes the FOD energy landscape. This sequence repeats seven times in this simple case until the global minimum is found. This behavior is commonly found in many optimization problems, but it can be particularly challenging in the case of finding optimal FODs due to the increased dimensionality for larger molecules, emphasizing the importance of developing reliable tools to determine initial FOD for the FLOSIC method.[42,43]

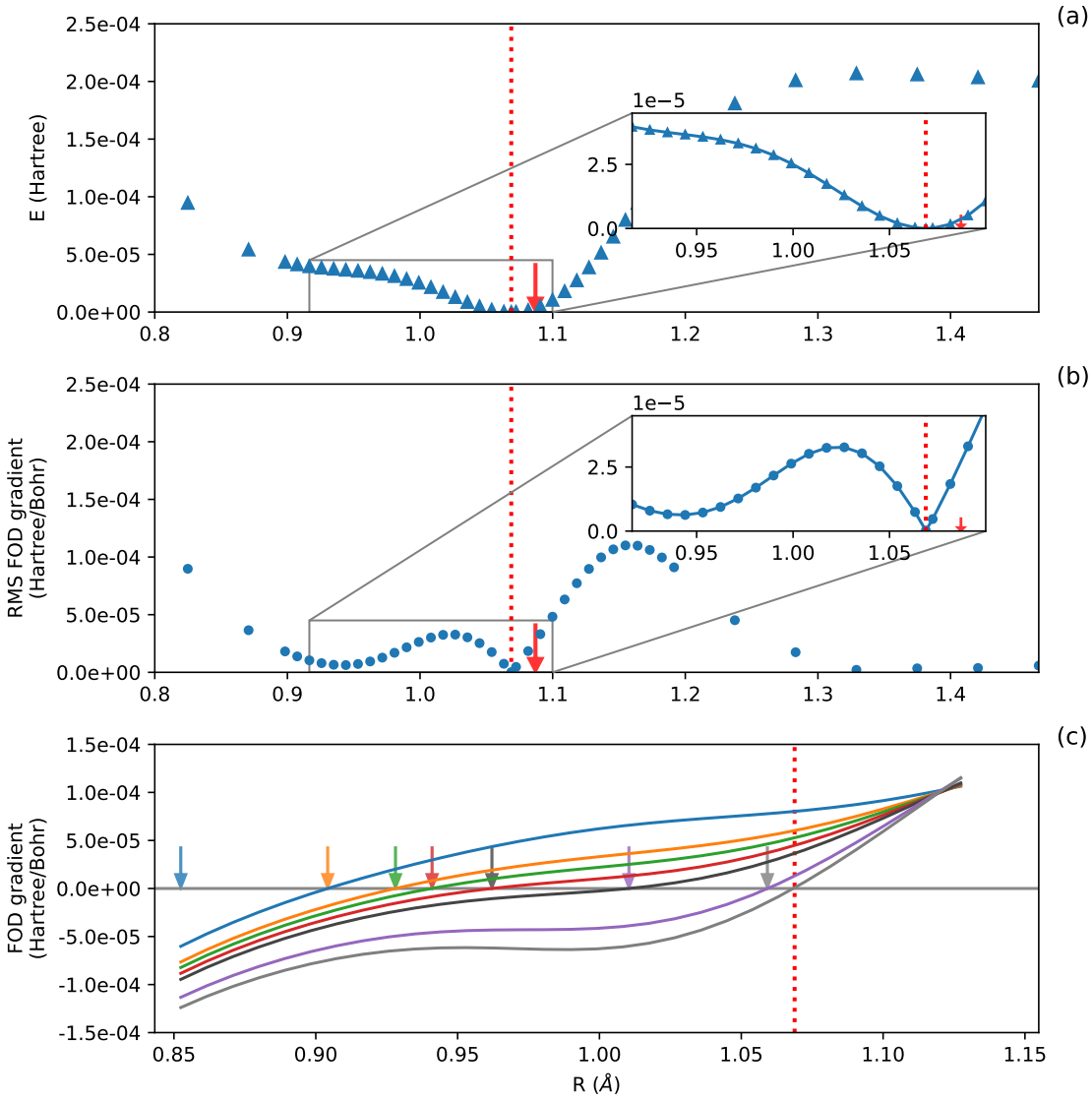

Figure 3: (a) Energy and (b) FOD gradient landscape for the FOD "breathing mode" for a methane molecule preserving T_d symmetry using the aug-cc-pVTZ basis and the LSDA functional. The red arrow in panels a and b indicate the FOD position for the calculation and the vertical red dotted line shows the global energy minimum. Panel c shows the FOD gradients for different FOD positions (represented with colored arrows) following an L-BFGS optimization sequence.

3. Applications

The FLOSIC method has been tested and benchmarked for a number of applications, including thermochemistry, and electrostatic and magnetic properties.[44–49] For the evaluation of many molecular properties, it is convenient to consider a small perturbation added to the total energy,

$$E(\mathbf{P}, \{\mathbf{a}\}) = E_{\mathrm{DFT}}(\mathbf{P}) + E_{\mathrm{SIC}}(\mathbf{P}, \{\mathbf{a}\}) + \lambda\Omega(\mathbf{P}), \tag{11}$$

and express the target property in terms of the second-order correction to the energy. In this case, $\lambda\frac{d\Omega}{d\mathbf{P}}$ represents the perturbative term to be added to the Hamiltonian, and λ is an infinitesimally small parameter. We show in the SI that since Ω does not depend on $\{\mathbf{a}\}$, the second-order in λ energy correction can be obtained at fixed FODs, i.e., the first-order response of the FOD with respect to the perturbation can be neglected:

$$E^{(2)} = \frac{d\Omega}{d\mathbf{P}} \cdot \frac{d\mathbf{P}}{d\lambda}\,. \tag{12}$$

For example, for the calculation of the (i, j) component of the electric dipole polarizability tensor, $\Omega_j(\mathbf{P}) = \langle x_j \rangle$, and $E^{(2)} = \langle \mathbf{R}_i \cdot \mathbf{P}_j^{(1)} \rangle$, where $\mathbf{R}_i$ is the i-component of the vector dipole matrix and $\mathbf{P}_j^{(1)}$ is the first-order density matrix corresponding to the electric field perturbation in the j direction, in analogy to standard linear-response theory. Obtaining $\mathbf{P}^{(1)}$, however, is not trivial as one would have to include the kernel response due to $E_{\mathrm{SIC}}(\mathbf{P}, a)$. While in practice, this has been done using finite perturbations (see for example Refs. 50–52), our results show that for the evaluation of second-order response properties, only the density needs to be relaxed, formally validating the use of a fixed FOD approach.

NMR properties are very sensitive to the underlying electronic structure method used for their evaluation, and thus removing self-interaction error is expected to have a significant effect. Using the Krieger-Li-Iafrate[53] approximation to the optimized effective potential for removing self-interaction error, Ziegler et al. have shown in an early paper[54] that self-

interaction can have a sizable impact on NMR shielding constants. Here we tested the effect of explicitly removing self-interaction error in an orbital-by-orbital basis using the FLOSIC method in a set of small molecules (CH_4, NH_3, N_2, and H_2O). To this end, we employed the LSDA and PBE functionals in combination with the aug-cc-pVQZ basis with the individual atomic centers as gauge origin. A self-consistency convergence threshold of 10^{-6} Ha in the energy and 10^{-8} in the RMS changes in the density matrix was used in all calculations for the SCF loop, and 10^{-6} Ha/Bohr in the RMS FOD forces for the FOD loop. FODs were relaxed using the same basis and the corresponding functional for each case (atomic coordinates and FODs are provided in the SI). Since E_{DFT} and E_{SIC} do not depend on the first-order paramagnetic current, the linear-response equations involved in the evaluation of the paramagnetic contribution are uncoupled and thus the paramagnetic term in the FLOSIC method can be evaluated as a simple sum-over-states. As a consistency check, we have tested the validity of this approach by comparing with explicit finite differences calculations of the paramagnetic contribution using a version of the code that works with complex density matrices (shown in the SI).

Table 1: Isotropic NMR shielding constants, σ, calculated with the FLOSIC method using the LSDA and PBE functionals (in ppm). The aug-cc-pVQZ basis is used with the gauge origin placed at each given nuclei. $\Delta = \sigma_{\mathrm{FLOSIC}} - \sigma_{\mathrm{DFT}}$

	LSDA			PBE		
	DFT	FLOSIC	Δ	DFT	FLOSIC	Δ
CH_4(C)	190.7	174.3	−16.4	188.0	168.1	−19.9
FH(F)	407.7	379.6	−28.1	403.2	374.0	−29.2
N_2(N)	−96.7	−104.9	−8.2	−88.0	−87.3	0.7
H_2O(O)	326.1	294.8	−31.3	320.1	281.2	−39.9
NH_3(N)	262.4	240.4	−22.0	257.7	217.9	−39.8

Table 1 shows the absolute NMR shielding constants for LSDA and PBE and their self-interaction corrected counterparts. In all cases, removing SIE leads to a shielding effect ($\Delta < 0$ in Table 1), shifting the NMR shielding constant towards a lower field region. The

diamagnetic contribution (not shown in Table 1) remains almost unaffected by removal of self-interaction error. This is somewhat expected since it is calculated as the expectation value of a short-range operator, and thus, unlike the dipole moment, it is less sensitive to subtle changes in the total density.[45,50,55] The effect of removing SIE in the isotropic NMR shielding constants is largely due to the change in the paramagnetic contribution. This contribution is negative in all cases, and becomes slightly larger in magnitude when SIE is removed using the FLOSIC method. This can be understood in terms of the slight reduction of the gap between the occupied and virtual orbitals that enter in the sum-over-states used to evaluate the paramagnetic contribution.

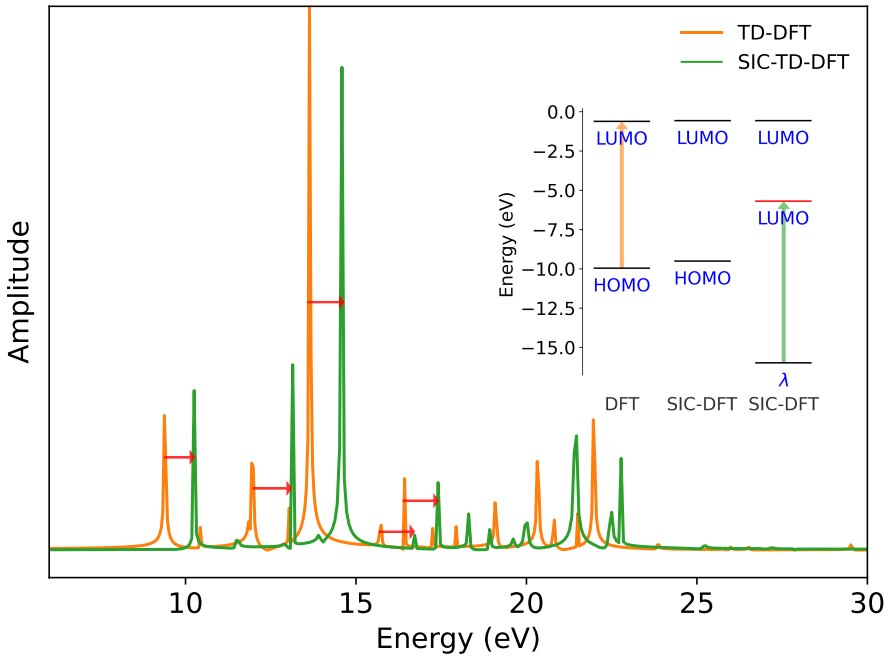

Figure 4: Excitation spectrum of the CH_4 molecule calculated from real-time TD-DFT propagation for DFT (orange) and self-interaction corrected DFT (green) using the FLOSIC method. The red arrows show the displacement of the main peaks. The inset shows the HOMO/LUMO energies as estimated from different methods. See text for details.

Since at convergence the effective $\mathbf{H}_{\mathrm{KS}}$ (eq. 7) satisfies the Roothaan equations for stationary (canonical) orbitals, it also satisfies the zero commutation relation between $\mathbf{H}_{\mathrm{KS}}$ and the total density matrix $\mathbf{P}$, which in the non-orthogonal AO representation takes the form $\mathbf{H}_{\mathrm{KS}}\mathbf{PS} - \mathbf{SPH}_{\mathrm{KS}} = \mathbf{0}$. In analogy to TD-DFT, one can thus write a Liouville–von Neumann

equation for the total time-dependent density matrix,

$$i\mathbf{S}\frac{d\mathbf{P}}{dt}\mathbf{S} = \mathbf{H}_{\mathrm{KS}}\mathbf{P}\mathbf{S} - \mathbf{S}\mathbf{P}\mathbf{H}_{\mathrm{KS}} \tag{13}$$

that includes the self-interaction correction in $\mathbf{H}_{\mathrm{KS}}$, and assumes that the FODs are kept fixed during the time evolution, which is formally justified if the deviation from equilibrium is small, as shown above. This approach provides a computationally costly but reliable way to obtain electronic excitations from self-interaction corrected DFT within the FLOSIC formalism. As a proof-of-concept, we used eq. 13 to perform a time dependent DFT (TD-DFT) propagation using the δ-kick method to determine the electronic excitation spectrum of the CH_4 molecule. The time propagation was carried out using a customary second-order Magnus expansion[56,57] with the second-order predictor-corrector scheme proposed by Cheng et al.[58] The total density matrix $\mathbf{P}$ as well as the single-orbital density matrices $\mathbf{P}_a$ are necessarily complex, while the FODs are kept real.[59,60] The calculations were performed using the aug-cc-pVTZ basis within the LSDA approximation as the underlying functional. A total propagation time of 90 fs and $5\,10^4$ time steps was used to allows for an energy resolution of approximately 0.07 eV. The excitation spectrum, calculated as the Fourier transform of the time-dependent dipole moment for the FLOSIC time-dependent density is shown in Figure 4 (the excitation spectrum for the Ne atom is shown in the SI).

Table 2: HOMO and LUMO energy levels (in eV) of the CH_4 molecule calculated with and without self-interaction correction using the LSDA functional and the aug-cc-pVTZ basis. The FLOSIC LUMO is evaluated by adding the first excitation energy from the TD-DFT calculation in Fig. 4 to the HOMO eigen-energy taken from the Lagrange multiplier matrix Λ. Reference values taken from Ref. 61.

	DFT	FLOSIC	Reference
HOMO	-10.0	-16.0	-13.6
LUMO	-0.6	-5.7	-2.7

The immediate feature that stands out in Figure 4 is a shift in the excitation peaks for the

FLOSIC energies towards higher frequencies of about 1 eV with respect to the non-corrected case (larger gap), in line with the expected physical effect of SIE removal.[62,63] In contrast, it is interesting to note that the HOMO and LUMO canonical energies resulting from the self-consistent FLOSIC calculation (obtained directly as the eigenvalues of $\mathbf{H}_{\mathrm{KS}}$) are not largely affected, and give only slightly smaller gap (see Table 2). In Perdew-Zunger (PZ), one can interpret the eigenvalues of the Lagrange multiplier matrix, Λ, utilized to solve the localization equations as the occupied orbital energies.[64] In FLOSIC, the Lagrange multiplier matrix is not directly involved in the calculation, but it can be easily constructed from $\frac{dE_{\mathrm{SIC}}}{d\mathbf{P}_a}$ in eq. 8 as $\Lambda_{ba} = \mathbf{X}_b \cdot \frac{dE_{\mathrm{SIC}}}{d\mathbf{P}_a} \cdot \mathbf{X}_a$[33,65] and leads to slightly asymmetric matrix at convergence. The eigenvalues of this matrix, after symmetrization (shown as λ in the inset of Fig. 4), can be interpreted as the occupied FLOSIC orbital energies, and turn out to be very close to those from the solution of the localization equations in traditional PZ.[66] However, virtual orbital energies are unaffected by the removal of SIE, giving an unphysical gap that is much larger than the actual gap. Our TD-DFT calculations provides a reliable estimation of this gap, which can be added to the HOMO value obtained from the symmetrized Lagrange multiplier matrix Λ. The resulting HOMO and LUMO for CH_4 is shown in Table 2. As discussed in Ref. 67 and references therein, there are other choices, including virtual-orbital dependent choices, that could be adopted depending on the application of interest. The strategy proposed in this work offers a robust estimation of the LUMO level (and potentially excitation energies) from FLOSIC calculations that can be used as reference for approximations that aim to estimate self-interaction corrected LUMO levels or excitation energies.

4. Summary

We provide a detailed workflow for the implementation of the FLOSIC method for removal of self-interaction error in DFT calculations in an orbital-by-orbital basis. The FLOSIC method effectively provides a transformation from M canonical orbitals to M localized Fermi-Löwdin

orbitals, determined by a set of M Fermi-orbital descriptors. This implementation takes advantage of the unitary invariant nature of the FLOSIC method to cast the self-consistent energy minimization at fixed Fermi-orbital descriptors in the same manner than standard Kohn-Sham with one additional term in the Kohn-Sham Hamiltonian that introduces the PZ self-interaction correction. Each energy minimization iteration is divided in two sub-steps, one for the density matrix and one for the Fermi-orbital descriptors. Expressions for the effective Kohn-Sham matrix and Fermi-orbital descriptor gradients are provided such that its implementation is suitable for most electronic structure codes. Moreover, the expression of the gradient of the total electronic energy, including SIC, with respect to the density matrix elements can be used in conjunction with the Fermi-orbital descriptor gradients and would allow for simultaneous relaxation of all variational parameters in FLOSIC calculations. Work along these lines is underway. We analyze the convergence characteristics of the algorithm and present applications for the evaluation of NMR shielding constants and real-time time-dependent DFT simulations based on the Liouville–von Neumann equation to calculate excitation energies.

Acknowledgement

This work was supported by the U.S. Department of Energy, Office of Science, Office of Basic Energy Sciences, as part of the Computational Chemical Sciences Program, under Award No. DE-SC0018331.

Supporting Information Available

Evaluation of the derivative of the $\mathbf{S}^{-1/2}$ matrix, derivation of eq. 11, comparison of analytic versus finite differences paramagnetic contribution to NMR shielding constants, excitation spectrum of the Ne atom, atomic coordinates and FODs positions, and basis set analysis for FOD relaxation and energy evaluation.

References

(1) Hohenberg, P.; Kohn, W. Inhomogeneous Electron Gas. *Phys. Rev.* **1964**, *136*, B864–B871.

(2) Kohn, W.; Sham, L. J. Self-Consistent Equations Including Exchange and Correlation Effects. *Phys. Rev.* **1965**, *140*, A1133–A1138.

(3) Postnikov, A. V.; Kortus, J.; Pederson, M. R. Density functional studies of molecular magnets. *Phys. Status Solidi B* **2006**, *243*, 2533–2572.

(4) Capelle, K. A Bird's-Eye View of Density-Functional Theory. *Braz. J. Phys.* **2006**, *36*, 1318–1343.

(5) Jensen, F. *Introduction to Computational Chemistry*, 2nd ed.; John Wiley & Sons: Chichester, 2007.

(6) Cramer, C. J.; Truhlar, D. G. Density functional theory for transition metals and transition metal chemistry. *Phys. Chem. Chem. Phys.* **2009**, *11*, 10757–10816.

(7) Jones, R. O. Density functional theory: Its origins, rise to prominence, and future. *Rev. Mod. Phys.* **2015**, *87*, 897–923.

(8) Li, C.; Zheng, X.; Su, N. Q.; Yang, W. Localized orbital scaling correction for systematic elimination of delocalization error in density functional approximations. *Natl. Sci. Rev.* **2018**, *5*, 203–215.

(9) Li, C.; Zheng, X.; Cohen, A. J.; Mori-Sánchez, P.; Yang, W. Local Scaling Correction for Reducing Delocalization Error in Density Functional Approximations. *Phys. Rev. Lett.* **2015**, *114*, 053001.

(10) Perdew, J. P. Density functional theory and the band gap problem. *Int. J. Quantum Chem.* **1985**, *28*, 497–523.

(11) Tu, G.; Carravetta, V.; Vahtras, O.; Agren, H. Core ionization potentials from self-interaction corrected Kohn-Sham orbital energies. *J. Chem. Phys.* **2007**, *127*, 174110.

(12) Hay, P. J.; Thibeault, J. C.; Hoffmann, R. Orbital interactions in metal dimer complexes. *J. Am. Chem. Soc* **1975**, *97*, 4884–4899.

(13) Perdew, J. P.; Zunger, A. Self-interaction correction to density-functional approximations for many-electron systems. *Phys. Rev. B* **1981**, *23*, 5048–5079.

(14) Pederson, M. R.; Lin, C. C. Localized and canonical atomic orbitals in self-interaction corrected local density functional approximation. *J. Chem. Phys.* **1988**, *88*, 1807–1817.

(15) Vydrov, O. A.; Scuseria, G. E. Ionization potentials and electron affinities in the Perdew–Zunger self-interaction corrected density-functional theory. *J. Chem. Phys.* **2005**, *122*, 184107.

(16) Vydrov, O. A.; Scuseria, G. E.; Perdew, J. P.; Ruzsinszky, A.; Csonka, G. I. Scaling down the Perdew-Zunger self-interaction correction in many-electron regions. *J. Chem. Phys.* **2006**, *124*, 094108.

(17) Vydrov, O. A.; Scuseria, G. E. Effect of the Perdew–Zunger self-interaction correction on the thermochemical performance of approximate density functionals. *J. Chem. Phys.* **2004**, *121*, 8187.

(18) Ruzsinszky, A.; Perdew, J. P.; Csonka, G. I.; Vydrov, O. A.; Scuseria, G. E. Spurious fractional charge on dissociated atoms: Pervasive and resilient self-interaction error of common density functionals. *J. Chem. Phys.* **2006**, *125*, 194112.

(19) Perdew, J. P.; Ruzsinszky, A.; Sun, J.; Pederson, M. R. *Advances In Atomic, Molecular, and Optical Physics*; Academic Press, 2015; Vol. 64; pp 1 – 14.

(20) Zope, R. R.; Yamamoto, Y.; Diaz, C. M.; Baruah, T.; Peralta, J. E.; Jackson, K. A.;

Santra, B.; Perdew, J. P. A step in the direction of resolving the paradox of Perdew-Zunger self-interaction correction. *J. Chem. Phys.* **2019**, *151*, 214108.

(21) Bhattarai, P.; Wagle, K.; Shahi, C.; Yamamoto, Y.; Romero, S.; Santra, B.; Zope, R. R.; Peralta, J. E.; Jackson, K. A.; Perdew, J. P. A step in the direction of resolving the paradox of Perdew–Zunger self-interaction correction. II. Gauge consistency of the energy density at three levels of approximation. *J. Chem. Phys.* **2020**, *152*, 214109.

(22) Zope, R. R.; Baruah, T.; Yamamoto, Y.; Basurto, L.; Díaz, C. M.; Peralta, J.; Jackson, K. A. FLOSIC code. `https://github.com/FLOSIC`, 2022; based on the NRLMOL code of M. R. Pederson.

(23) Pederson, M. R. Fermi orbital derivatives in self-interaction corrected density functional theory: Applications to closed shell atoms. *J. Chem. Phys.* **2015**, *142*, 064112.

(24) Yang, Z.; Pederson, M. R.; Perdew, J. P. Full self-consistency in the Fermi-orbital self-interaction correction. *Phys. Rev. A* **2017**, *95*, 052505.

(25) Pederson, M. R.; Ruzsinszky, A.; Perdew, J. P. Communication: Self-interaction correction with unitary invariance in density functional theory. *J. Chem. Phys.* **2014**, *140*, 121103.

(26) Löwdin, P.-O. The nonorthogonality problem connected with the use of atomic wave functions in the theory of molecules and crystals. *J. Chem. Phys.* **1950**, *18*, 365–375.

(27) Zope, R. R.; Baruah, T.; Yamamoto, Y.; Basurto, L.; Díaz, C. M.; Peralta, J.; Jackson, K. A. FLOSIC. based on the NRLMOL code of M. R. Pederson.

(28) Foster, J. M.; Boys, S. F. Canonical Configurational Interaction Procedure. *Rev. Mod. Phys.* **1960**, *32*, 300–302.

(29) Boys, S. F. Construction of Some Molecular Orbitals to Be Approximately Invariant for Changes from One Molecule to Another. *Rev. Mod. Phys.* **1960**, *32*, 296–299.

(30) Edmiston, C.; Ruedenberg, K. Localized Atomic and Molecular Orbitals. *Rev. Mod. Phys.* **1963**, *35*, 457–464.

(31) Pipek, J.; Mezey, P. G. A fast intrinsic localization procedure applicable for ab initio and semiempirical linear combination of atomic orbital wave functions. *J. Chem. Phys.* **1989**, *90*, 4916–4926.

(32) Schwalbe, S.; Fiedler, L.; Kraus, J.; Kortus, J.; Trepte, K.; Lehtola, S. PyFLOSIC: Python-based Fermi–Löwdin orbital self-interaction correction. *J. Chem. Phys.* **2020**, *153*, 084104.

(33) Aquino, F. W.; Wong, B. M. Additional Insights between Fermi–Löwdin Orbital SIC and the Localization Equation Constraints in SIC-DFT. *J. Phys. Chem. Lett.* **2018**, *9*, 6456–6462.

(34) Shinde, R.; Yamijala, S. S. R. K. C.; Wong, B. M. Improved band gaps and structural properties from Wannier–Fermi–Löwdin self-interaction corrections for periodic systems. *J. Phys. Cond. Matter* **2021**, *33*, 115501.

(35) Diaz, C. M.; Suryanarayana, P.; Xu, Q.; Baruah, T.; Pask, J. E.; Zope, R. R. Implementation of Perdew–Zunger self-interaction correction in real space using Fermi–Löwdin orbitals. *J. Chem. Phys.* **2021**, *154*, 084112.

(36) Diaz, C. M.; Baruah, T.; Zope, R. R. Fermi-Löwdin-orbital self-interaction correction using the optimized-effective-potential method within the Krieger-Li-Iafrate approximation. *Phys. Rev. A* **2021**, *103*, 042811.

(37) Mayer, I. On Löwdin's method of symmetric orthogonalization. *Int. J. Quantum Chem.* **2002**, *90*, 63–65.

(38) Pederson, M. R.; Baruah, T. Self-Interaction Corrections Within the Fermi-Orbital-Based Formalism. *Adv. At. Mol. Opt. Phys.* **2015**, *64*, 153.

(39) Lehtola, S.; Jónsson, H. Variational, Self-Consistent Implementation of the Perdew-Zunger Self-Interaction Correction with Complex Optimal Orbitals. *J. Chem. Theory Comput.* **2014**, *10*, 5324–5337.

(40) Cheng, L.; Gauss, J. Analytic energy gradients for the spin-free exact two-component theory using an exact block diagonalization for the one-electron Dirac Hamiltonian. *J. Chem. Phys.* **2011**, *135*, 084114.

(41) Frisch, M. J.; Trucks, G. W.; Schlegel, H. B.; Scuseria, G. E.; Robb, M. A.; Cheeseman, J. R.; Scalmani, G.; Barone, V.; Petersson, G. A.; Nakatsuji, H.; Li, X.; Caricato, M.; Marenich, A. V.; Bloino, J.; Janesko, B. G.; Gomperts, R.; Mennucci, B.; Hratchian, H. P.; Ortiz, J. V.; Izmaylov, A. F.; Sonnenberg, J. L.; Williams-Young, D.; Ding, F.; Lipparini, F.; Egidi, F.; Goings, J.; Peng, B.; Petrone, A.; Henderson, T.; Ranasinghe, D.; Zakrzewski, V. G.; Gao, J.; Rega, N.; Zheng, G.; Liang, W.; Hada, M.; Ehara, M.; Toyota, K.; Fukuda, R.; Hasegawa, J.; Ishida, M.; Nakajima, T.; Honda, Y.; Kitao, O.; Nakai, H.; Vreven, T.; Throssell, K.; Montgomery, J. A., Jr.; Peralta, J. E.; Ogliaro, F.; Bearpark, M. J.; Heyd, J. J.; Brothers, E. N.; Kudin, K. N.; Staroverov, V. N.; Keith, T. A.; Kobayashi, R.; Normand, J.; Raghavachari, K.; Rendell, A. P.; Burant, J. C.; Iyengar, S. S.; Tomasi, J.; Cossi, M.; Millam, J. M.; Klene, M.; Adamo, C.; Cammi, R.; Ochterski, J. W.; Martin, R. L.; Morokuma, K.; Farkas, O.; Foresman, J. B.; Fox, D. J. Gaussian16 Revision C.01. 2016; Gaussian Inc. Wallingford CT.

(42) Nguyen, D. B.; Pederson, M. R.; Perdew, J. P.; Jackson, K. A.; Peralta, J. E. Initial Fermi orbital descriptors for FLOSIC calculations: The quick-FOD method. *Chem. Phys. Lett.* **2021**, *780*, 138952.

(43) Schwalbe, S.; Trepte, K.; Fiedler, L.; Johnson, A. I.; Kraus, J.; Hahn, T.; Peralta, J. E.; Jackson, K. A.; Kortus, J. Interpretation and Automatic Generation of Fermi-Orbital Descriptors. *J. Comp. Chem.* **2019**, *40*, 2843–2857.

(44) Sharkas, K.; Li, L.; Trepte, K.; Withanage, K. P. K.; Joshi, R. P.; Zope, R. R.; Baruah, T.; Johnson, J. K.; Jackson, K. A.; Peralta, J. E. Shrinking Self-Interaction Errors with the Fermi–Löwdin Orbital Self-Interaction-Corrected Density Functional Approximation. *J. Phys. Chem. A* **2018**, *122*, 9307–9315.

(45) Johnson, A. I.; Withanage, K. P.; Sharkas, K.; Yamamoto, Y.; Baruah, T.; Zope, R. R.; Peralta, J. E.; Jackson, K. A. The effect of self-interaction error on electrostatic dipoles calculated using density functional theory. *J. Chem. Phys.* **2019**, *151*, 174106.

(46) Joshi, R. P.; Trepte, K.; Withanage, K. P. K.; Sharkas, K.; Yamamoto, Y.; Basurto, L.; Zope, R. R.; Baruah, T.; Jackson, K. A.; Peralta, J. E. Fermi-Löwdin Orbital Self-interaction Correction to Magnetic Exchange Couplings. *J. Chem. Phys.* **2018**, *149*, 164101.

(47) Sharkas, K.; Wagle, K.; Santra, B.; Akter, S.; Zope, R. R.; Baruah, T.; Jackson, K. A.; Perdew, J. P.; Peralta, J. E. Self-interaction error overbinds water clusters but cancels in structural energy differences. *Proc. Natl. Acad. Sci.* **2020**, *117*, 11283–11288.

(48) Vargas, J.; Ufondu, P.; Baruah, T.; Yamamoto, Y.; Jackson, K. A.; Zope, R. R. Importance of self-interaction-error removal in density functional calculations on water cluster anions. *Phys. Chem. Chem. Phys.* **2020**, *22*, 3789–3799.

(49) Withanage, K. P. K.; Sharkas, K.; Johnson, J. K.; Perdew, J. P.; Peralta, J. E.; Jackson, K. A. Fermi–Löwdin orbital self-interaction correction of adsorption energies on transition metal ions. *J. Chem. Phys.* **2022**, *156*, 134102.

(50) Withanage, K. P. K.; Akter, S.; Shahi, C.; Joshi, R. P.; Diaz, C.; Yamamoto, Y.; Zope, R.; Baruah, T.; Perdew, J. P.; Peralta, J. E.; Jackson, K. A. Self-interaction-free electric dipole polarizabilities for atoms and their ions using the Fermi-Löwdin self-interaction correction. *Phys. Rev. A* **2019**, *100*, 012505.

(51) Akter, S.; Yamamoto, Y.; Zope, R. R.; Baruah, T. Static dipole polarizabilities of polyacenes using self-interaction-corrected density functional approximations. *J. Chem. Phys.* **2021**, *154*, 114305.

(52) Akter, S.; Yamamoto, Y.; Diaz, C. M.; Jackson, K. A.; Zope, R. R.; Baruah, T. Study of self-interaction errors in density functional predictions of dipole polarizabilities and ionization energies of water clusters using Perdew–Zunger and locally scaled self-interaction corrected methods. *J. Chem. Phys.* **2020**, *153*, 164304.

(53) Krieger, J. B.; Li, Y.; Iafrate, G. J. Systematic approximations to the optimized effective potential: Application to orbital-density-functional theory. *Phys. Rev. A* **1992**, *46*, 5453–5458.

(54) Patchkovskii, S.; Autschbach, J.; Ziegler, T. Curing difficult cases in magnetic properties prediction with self-interaction corrected density functional theory. *J. Chem. Phys.* **2001**, *115*, 26–42.

(55) Helgaker, T.; Jaszuński, M.; Ruud, K. Ab Initio Methods for the Calculation of NMR Shielding and Indirect Spin-Spin Coupling Constants. *Chem. Rev.* **1999**, *99*, 293–352.

(56) Magnus, W. On the exponential solution of differential equations for a linear operator. *Comm. Pure Appl. Math.* **1954**, *7*, 649–673.

(57) Castro, A.; Marques, M. A. L.; Rubio, A. Propagators for the time-dependent Kohn–Sham equations. *J. Chem. Phys.* **2004**, *121*, 3425–3433.

(58) Cheng, C.-L.; Evans, J. S.; Van Voorhis, T. Simulating molecular conductance using real-time density functional theory. *Phys. Rev. B* **2006**, *74*, 155112.

(59) Lehtola, S.; Head-Gordon, M.; Jónsson, H. Complex Orbitals, Multiple Local Minima, and Symmetry Breaking in Perdew-Zunger Self-Interaction Corrected Density Functional Theory Calculations. *J. Chem. Theory Comput.* **2016**, *12*, 3195–3207.

(60) Withanage, K. P. K.; Jackson, K. A.; Pederson, M. R. Complex Fermi–Löwdin orbital self-interaction correction. *J. Chem. Phys.* **2022**, *156*, 231103.

(61) Zhang, G.; Musgrave, C. B. Comparison of DFT Methods for Molecular Orbital Eigenvalue Calculations. *J. Phys. Chem. A* **2007**, *111*, 1554–1561, PMID: 17279730.

(62) Zeng, T.; He, Y. Scaling of the self-energy correction to the HOMO-LUMO gap with magnesium cluster size and its potential for extrapolating to larger magnesium clusters. *J. App. Phys.* **2018**, *124*, 044305.

(63) Diaz, C. M.; Basurto, L.; Adhikari, S.; Yamamoto, Y.; Ruzsinszky, A.; Baruah, T.; Zope, R. R. Self-interaction-corrected Kohn–Sham effective potentials using the density-consistent effective potential method. *J. Chem. Phys.* **2021**, *155*, 064109.

(64) Pederson, M. R.; Heaton, R. A.; Lin, C. C. Density-functional theory with self-interaction correction: Application to the lithium molecule). *J. Chem. Phys.* **1985**, *82*, 2688–2699.

(65) Jackson, K. A.; Withanage, K. P. K.; Peralta, J. E. Comment: "Additional Insights between Fermi- Löwdin Orbital SIC and the Localization Equation Constraints in SIC-DFT". *J. Phys. Chem.* **2019**, *123*, 4322.

(66) Kao, D.-y.; Withanage, K.; Hahn, T.; Batool, J.; Kortus, J.; Jackson, K. Self-consistent self-interaction corrected density functional theory calculations for atoms using Fermi-Löwdin orbitals: Optimized Fermi-orbital descriptors for Li–Kr. *J. Chem. Phys.* **2017**, *147*, 164107.

(67) Baruah, T.; Pederson, M. R. DFT Calculations on Charge-Transfer States of a Carotenoid-Porphyrin-C60 Molecular Triad. *J. Chem. Theory Comput.* **2009**, *5*, 834–843, PMID: 26609590.

Graphical TOC Entry